Cylindrical cam mechanism for unlimited subsequent spring recruitment in Series-Parallel Elastic Actuators

Mathijssen, Glenn; Furnemont, Raphaël; Verstraten, Tom; Lefeber, Dirk; Vanderborght, Bram

Published in:
2015 IEEE International Conference on Robotics and Automation (ICRA)

DOI:
10.1109/ICRA.2015.7139278

Publication date:
2015

Document Version:
Accepted author manuscript

Cylindrical cam mechanism for unlimited subsequent spring recruitment in Series-Parallel Elastic Actuators

Glenn Mathijssen[1,2*], Raphaël Furnémont[1], Simon Beckers[1], Tom Verstraten[1], Dirk Lefeber[1], and Bram Vanderborght[1]

***Abstract*— Series-Parallel Elastic Actuators (SPEA) enable variable recruitment of parallel springs and variable load cancellation. In previous work, we validated a MACCEPA-based SPEA prototype with a self-closing intermittent mechanism, to reduce motor load and improve energy efficiency. However, the mechanism only allowed for 4 parallel springs and a limited equilibrium angle range, which limits the variable load cancellation and operation range. Therefore, we developed a novel cylindrical cam mechanism for unlimited subsequent spring recruitment. This paper describes and validates the working principle of the cylindrical cam mechanism. Furthermore, the latest MACCEPA-based SPEA is presented with a maximum output torque of 40 Nm and variable stiffness. Additive and traditional manufacturing techniques go hand in hand to overcome the actuator's complexity. The experiments endorse the working principle, demonstrate the variable stiffness, and prove the motor torque can be reduced to 5 Nm while an output torque of 40 Nm can be achieved.**

I. INTRODUCTION

Compliant actuators have been developing rapidly in the robotics community for about 2 decades. The Series Elastic Actuator (SEA) introduced a compliant element, typically a spring, in series of a traditional servomotor. Inspired by human's ability to alter the joint stiffness by co-contracting antagonistic muscles, the Variable Stiffness Actuator (VSA) introduced the possibility to alter the joint stiffness. More recently, Variable Impedance Actuators (VIA) have been introduced, which allow to also change the damping of a joint. The interested reader can consult the recent review [1] on VIA for further information.

The main virtues of compliant actuators are threefold. Firstly, they offer increased safety and robustness by decoupling the inertia over the spring [2] [3] [4]. Moreover, shocks can be absorbed due to the very high (virtually infinite) bandwidth of the passive compliant element. Secondly, impedance control can be performed by inexpensive measurement of the spring's deformation. Thirdly, compliant actuators increase the energy efficiency by storing and recoiling energy through the spring [5] [6] [7]. The latter is, however, limited to cyclic motions that include phases of negative power, and to power bursts to release stored energy instantly [8].

*This work was supported in part by the ERC-grant SPEAR (no.337596). Tom Verstraten and Glenn Mathijssen are funded by PhD Fellowship of the Research Foundation - Flanders (FWO).

[1] Robotics & Multibody Mechanics Research Group, Faculty of Mechanical Engineering, Vrije Universiteit Brussel, 1050 Elsene, Belgium. http://mech.vub.ac.be/robotics

[2] Interdepartemental Research Centre E. Piaggio, Faculty of Engineering, University of Pisa. http://www.centropiaggio.unipi.it/

* Corresponding author: glenn.mathijssen@vub.ac.be

As we described in [9], an important downside of the current VIA designs is the proportional relationship between the output load and the motor load due to their serial designs. A gear train is typically installed to decrease the output load with respect to the motor side. However, this drastically increases the energy losses and the weight of the actuator. Furthermore, increased output loads still result in increased motor loads, which result in continuous (copper) losses, even at low speeds and thus low mechanical output power. One way is to design counterbalance mechanisms such as for the service robot arm of [10]. Numerous recent efforts attempt to push the boundaries of current actuators such as for example Paine et al. [11], Tsagarakis et al. [12] and Urata et al. [13]. Nonetheless, actuators with a high torque to weight ratio and high energy efficiency remain a challenge for the robotics community. In order to address these challenges, we proposed the novel Series Parallel Elastic Actuator (SPEA) with multiple springs in parallel, which can be recruited subsequently by dephased intermittent mechanisms in parallel. Our first prototype based on mutilated gears proved the underlying SPEA principles and showed practical feasibility [14]. The experiments showed that the motor torque T_{motor} can be reduced by approximately the number of parallel springs and the energy required is only 11% compared to a SEA. It is important to notice that in the remainder of this paper, T_{motor} is the torque after the motor and the geartrain. In order to provide bi-directional output torque, variable stiffness, and a more reliable locking mechanism, we proposed and presented an improved SPEA in [15], based on our in-house designed VSA MACCEPA (The Mechanically Adjustable Compliance and Controllable Equilibrium Position Actuator) [16]. In [15] the self-closing mechanism is modeled and tested, and a first MACCEPA-based SPEA prototype is presented.

A significant limitation of the MACCEPA-based SPEA as presented in [15] is the limited number of springs in parallel and the limited output equilibrium angle. The general MACCEPA-based SPEA principle and the limitations will be further depicted in section II. In section III an innovative cylindrical cam mechanism is presented for unlimited subsequent spring recruitment and increased output equilibrium angle. The MACCEPA-based SPEA of [15] has an output torque limited to 2 Nm. As will be shown in section IV the MACCEPA-based SPEA presented in this paper provides an output torque of 40 Nm. Moreover, section IV discusses how the combination of traditional and additive manufacturing techniques allow to overcome the complexity of the actuator.

The experiments presented in section V show the working principle of the MACCEPA-based SPEA with cylindrical cam mechanism, the lowered motor torque and the variable stiffness. Section VI concludes the paper and discusses future work.

II. MACCEPA-BASED SPEA AND CURRENT LIMITATIONS

The original MACCEPA design [16] is shown in Fig. 1a. It consists of a motor, fixed to the ground link, which actuates a lever arm (red) of length B that rotates around the joint axis. A spring is connected to the lever arm and to the output link. The equilibrium position φ is the position where T_{output}=0. The output torque T_{output} is a function of the deviation angle α. By increasing the pretension P of the spring with a second motor, the stiffness of the joint can be independently varied. Since only a single linear spring is required, the MACCEPA allows for a straight-forward non-complex design. In [15] we presented a novel altered MACCEPA that enables to disconnect the motor arm (red) from the spring when the motor arm angle $|\omega|$ exceeds φ_{end}. The tensioner (green) then locks the spring at φ_{end} of the guide (blue) as presented in Fig. 1b. Henceforth, the motor arm angle is defined as ω and the equilibrium angle φ. As such, this results in an intermittent mechanism which can be expressed as (1). Figures 1c, 1d and 1e show the newly presented aluminum guide, tensioner and motor arm.

$$\varphi = \begin{cases} \varphi_{end} & \omega > \varphi_{end} \\ \omega \quad if & |\omega| \leq \varphi_{end} \\ -\varphi_{end} & \omega < -\varphi_{end} \end{cases} \tag{1}$$

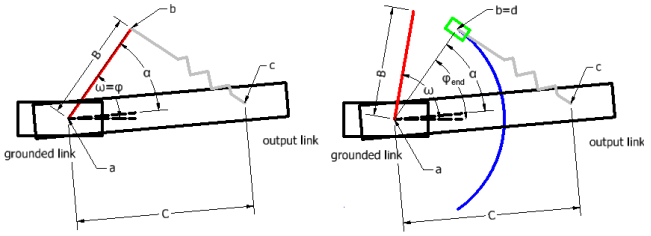

(a) The original MACCEPA. (b) Novel MACCEPA + guide (blue).

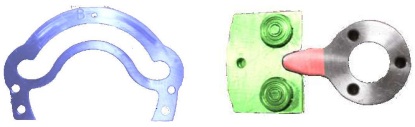

(c) Self-closing guide.

(d) Tensioner and motor arm.

(e) Self-closing mechanism.

Fig. 1. Schematic and nomenclature of the original (a) and novel (b) MACCEPA. Guide in blue, tensioner in green and lever arm in red. The guide (c) and, tensioner and motor arm (d) form the self-closing mechanism (e). In (e) the tensioner is locked at the extremity of the self-closing guide.

Full details regarding the parametrization and model of the curvature of the guide, accompanied by experimental verifications, can be found in [15]. The difference in this work is that the components are produced in aluminum to increase the actuator's performance. The forces expected in the components are an order of magnitude higher than in [15]. First, the experiment with the improved components is shown in Fig. 2, which reaffirms the working principle of the self-closing mechanism. The measured motor torque T_{motor} clearly follows the modeled trend in Fig. 2, including the required locking torque at both extremities of the self closing guide. The output torque T_{output} generated by 1 layer reaches 3.5 Nm for 5% pretension. The ellipses indicate that after locking the spring at φ_{end}, the motor torque drops to 0 Nm, which results in load cancellation since T_{output} is preserved.

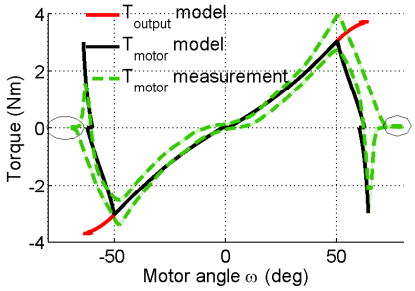

Fig. 2. The measured T_{motor} (green) to position a spring from one side of the guide to the other, and in reverse, clearly matches the modeled trend (black). T_{output} reaches 3.5 Nm for 5% pretension.

The working principle of the MACCEPA-based SPEA is based on multiple parallel layers of the modified MACCEPA with self-closing mechanism. As indicated in Fig. 3a, the maximum equilibrium position $\pm\varphi_{max}$ can be reached by positioning all parallel springs at $\pm\varphi_{end}$. The neutral position $\varphi = 0$ can be reached by positioning half of the springs on each side as shown in Fig. 3b. In [15] only four parallel layers are installed with an equilibrium angle range [-45^o,45^o]. The main limitation in this design lies in the the fact that all four motor arms are fixed to the motor shaft, and dephased mutually. After locking the first spring, the first motor arm will collide with its tensioner after approximately 360^o. This is indicated in Fig. 3c where the motor arm (red) is shown during 360^o travel of the motor shaft. As such, the maximum dephasing between the motor arms is approximately $\frac{360}{\#layers}$, which directly limits the range of φ. The main novelty in this work is the cylindrical cam mechanism presented in section III which ensures the actuator can consist of an unlimited number of parallel layers without limiting the range of φ. The range of φ for the self-closing guide in Fig. 1c is [-60^o,60^o].

III. WORKING PRINCIPLE MACCEPA-BASED SPEA WITH CYLINDRICAL CAM MECHANISM

Cylindrical cam mechanisms, and cam mechanisms in general, have been used for centuries to convert a certain input profile to a desired output profile. An extensive collection of cam-based mechanisms can be found for example in [17]. One of the uses in recent robotic research is to deploy cam mechanisms to store and release energy in spring mechanisms. For example in a recent walking and jumping robot [18], a cylindrical cam-mechanism is used to store

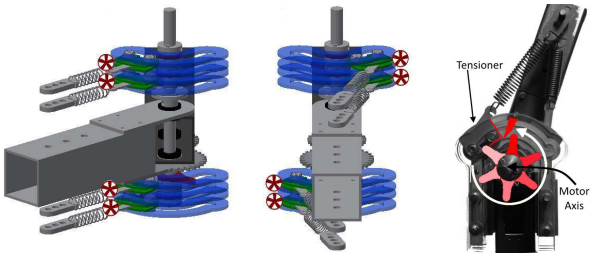

(a) Maximum equilibrium angle φ_{max}. (b) Neutral position. (c) Motor arm collision after 360^0.

Fig. 3. By positioning the tensioners (indicated by the red stars), the equilibrium position of the MACCEPA-based SPEA can be altered. In (a) the maximum equilibrium angle is achieved, while for (b) the equilibrium angle is 0^o. From (c) it is clear that the motor arm will collide with its tensioner after approximately 360^o.

energy in a spring by continuous rotation of a motor shaft and automatically releasing this energy to jump. Also in [19] cam discs and cam rollers are used in a VSA.

In this work a cylindrical cam mechanism is devised as an intermittent mechanism. The main idea is explained in Fig. 4. The motor arm (red) is fixed to the cylindrical cam mechanism (orange), which is journaled for rotation with respect to the splined motor shaft (brown) by means of a bushing. During 180^o rotation of the motor shaft, the lever arm stays *in plane* (i.e. perpendicular to the motor shaft) so that it can recruit the spring of a certain actuation layer. During this period the motor torque will be similar to the one discussed in Fig. 2. During the next 180^o, the cam follower (gray) enters the groove of the cylindrical cam mechanism. As a result, the motor arm moves *out of its plane* (i.e. parallel to the motor shaft) in order to reposition to the next parallel actuation layer. The two phases are further respectively referred to as *actuation phase* and *travel phase*, and indicated on Fig. 4 by a curved double arrow and a straight double arrow. From Fig. 4a to 4d the motor shaft turns 360^o and both motor arms go through an actuation and travel phase, though both shifted. By comparing Fig. 4a and 4d it is clear that both lever arms recruited one spring (one actuation phase) and traveled one layer upwards (one travel phase). This innovative mechanism is the key for unlimited subsequent spring recruitment in a MACCEPA-based SPEA.

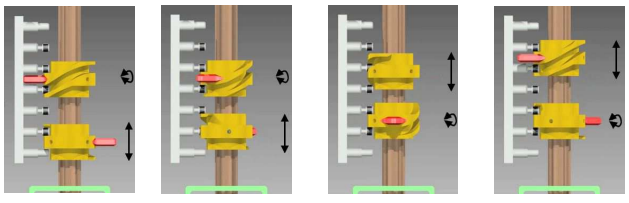

(a) 0^o (b) 120^o (c) 240^o. (d) 360^o.

Fig. 4. By continuous motor shaft rotation each motor arm, attached to a cylindrical cam mechanism, will recruit one spring (curved arrow) and be positioned to recruit the next spring (straight arrow). Please watch the attached video file for extra clarification.

The cylindrical cam groove is designed to have continuous first and second derivatives of displacement across the entire groove, while the jerk remains finite. As such, the shocks on cam follower and cam groove are minimized. A 7 degree of freedom (DOF) polynomial was chosen which resulted in a so called 4-5-6-7 curve (since first 4 constants become zero). Figure 5a shows the unfolded cylindrical cam groove and Fig. 5b the full cylindrical cam with fixed motor arm.

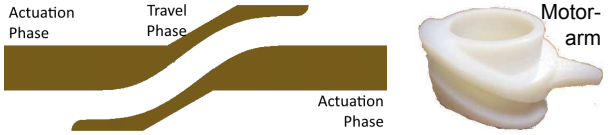

(a) Unfolded 4-5-6-7 curve. (b) Picture of cam.

Fig. 5. The cylindrical cam mechanisms with fixed motor arm are printed with PolyJet prototyping technology of Materialise ©, Belgium.

The self-closing guides provide reliable locking up to an output angle range of [-60^o,60^o]. This means that a spring can be recruited over 120^o while so far an actuation phase of 180^o is assumed. The travel phase indeed ends after 180^o. Next, during 30^o the cam already turns in plane before really recruiting a spring. After the 120^o recruitment, the cam again turns 30^o in plane without recruiting a spring. In case only two cams are installed, which are dephased 180^o, then there is no bijection between motor angle ω and equilibrium angle φ, due to the 2 phases of 30^o in plane without recruiting. In order to ensure the bijection, 2 consecutive actuation phases have a 30^o overlap and the complete set-up consists of 4 cylindrical cam mechanisms. With this set-up, which is shown in Fig. 7a, the goal of unlimited subsequent spring recruitment is achieved. An animation to clarify this innovative solution is given in the supplementary video. This design allows for a modular design of parallel SPEA layers since extra layers can be added without altering the mechanism itself.

IV. ACTUATOR DESIGN AND SPECIFICATIONS

The final MACCEPA-based SPEA with cylindrical cam mechanism consists of 8 parallel springs and is presented in Fig. 6. The recruitment mechanism (left of the springs) and the non-backdrivable pretensioning mechanism (right of the springs) are discussed in detail in respectively section IV-A and section IV-B.

Fig. 6. The final MACCEPA-based SPEA with cylindrical cam mechanism. On the left the motor and cylindrical cam mechanism and self-closing guides. On the right the pretensioning mechanism for variable stiffness.

A. Recruitment mechanism

Since the number of components increases in a SPEA due to the layers in parallel, the complexity of the actuator

increases as well. In order to overcome this increased complexity in the recruitment mechanism, traditional and additive manufacturing techniques are combined to profit from the virtues of both. This combination proved successful for both the cylindrical cams and the guide holder.

The cylindrical cams, as shown in Fig. 5, are a complex shape requiring 4-axis CNC machines which are not always commonly available. However, since one of the 8 parallel springs only requires approximately $\frac{1}{8}$ of the output force/torque during recruitment, it is still possible to produce the cams (including motor arm) by additive manufacturing. Furthermore, compared to CNC machining the lead time is several times shorter and the price more than an order of magnitude lower. The cams are produced by Materialise ©, Belgium and printed in high detail resin with PolyJet prototyping technology (tensile strength 49,8 MPa and impact resistance 37,5 $\frac{KJ}{mm^2}$). The ultra thin layers ensure a smooth groove. A finite element analysis showed a maximum of 25 MPa Von Mises Stress on the motor arm. The splined steel axis is 14 mm in diameter and has compatible bronze bushings. The printed cams are then fixed to the bushings by set screws. The needle cam followers (IKO/Nippon Thompson ©) are 5 mm in outer diameter. One could expect friction losses in the bushing during the travel phase. However, since during this phase there is no load on the motor arm, the friction losses are negligible.

The guides and tensioners are CNC machined in aluminum, while the guide holder is printed in Alumide via laser sintering by Materialise ©, Belgium. Alumide is a blend of aluminum powder and polyamide power. Again this combination proves successful. The CNC machined parts are non-complex but strong. The load is then transferred to the guide holder which is a highly complex part where the guides match in. The precision of the laser sintering (up to 0.12 mm) is sufficient for the guide holder to act as a mold where the guides are positioned correctly. Two aluminum covers on top and bottom of the guide holder are added with bearing for the motor shaft as well. Two excessive aluminum supports are added for rigidity since the guide holder is printed with a wall thickness of 3 mm. Based on finite element analysis it is expected that these supports can be omitted in a future version when the guide holder is solid.

The motor is a Maxon ©DCX 22L with GPX 22 gearbox of 1:62 ratio, 74% maximum efficiency and 0.165 kg weight. Inside the ground link a belt transmission of 1:4 is installed to reach 5.2 Nm continuous, as indicated in Fig. 6. The motor is positioned outside the guide holder for demonstration purposes. The springs are challenging since the outside diameter can only be 10 mm while the maximum extension is around 100 mm. As such, the rest length of standard extension springs increases. The installed springs are Tevema ©T32079 springs with an outer diameter of 9.6 mm and stiffness 1.7 N/mm.

B. Pretensioning mechanism

The pretensioning mechanism is designed to pretension all the springs at once. The aim is not to change the stiffness dynamically during runs but only when switching operation mode [5]. Since the equilibrium angle and pretension are independent in the MACCEPA, the pretensioning motor can be downsized. As shown in Fig.8a the Cevlar cables of the springs are connected to a reeling rod. This reeling rod is driven by a wormwheel (ratio 1:40), of which the worm is driven by a SAVOX 0251 MG servomotor. The wormwheel is positioned inside the output link and supports with bearings for the reeling rod are added as shown in Fig.8c. Since the pretension is only changed between runs and not dynamically during runs, the non-backdrivable worm drive is highly useful to avoid wasting copper losses in the servomotor. The bearings included in the worm drive account for the trust forces.

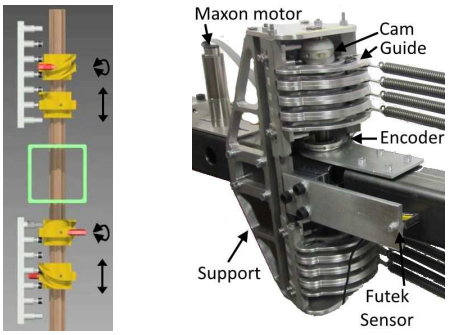

(a) Cam mechanism. (b) Realization of the recruitment mechanism.

Fig. 7. The recruitment mechanism is a combination of additive and traditional manufacturing techniques.

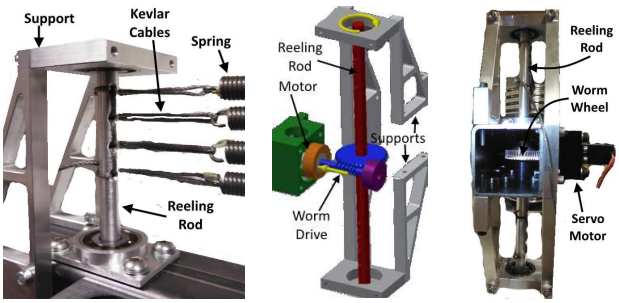

(a) Close-up of reeling rod and kevlar cables. (b) CAD drawing. (c) Pretension drive train.

Fig. 8. The pretensioning mechanism is designed to pretension all springs and lock the pretensioning by means of a non-backdrivable mechanism.

C. The final MACCEPA-based SPEA with cylindrical cam mechanism

The complete actuator has a weight of 2.2 kg. This can be reduced in an improved version to approximately 1.5 kg. Firstly, the supports are too rugged. Secondly, each layer currently consists of 2 guides, which can be reduced to 1 guide in an altered design. The latter will also reduce the height of the actuator from currently 200 mm (not including the central link) to 175 mm. The maximum T_{output} is 30 Nm at the neutral position and 40 Nm where the deflection angle is 90^o. Since an actuator with limited power rating (20 W)

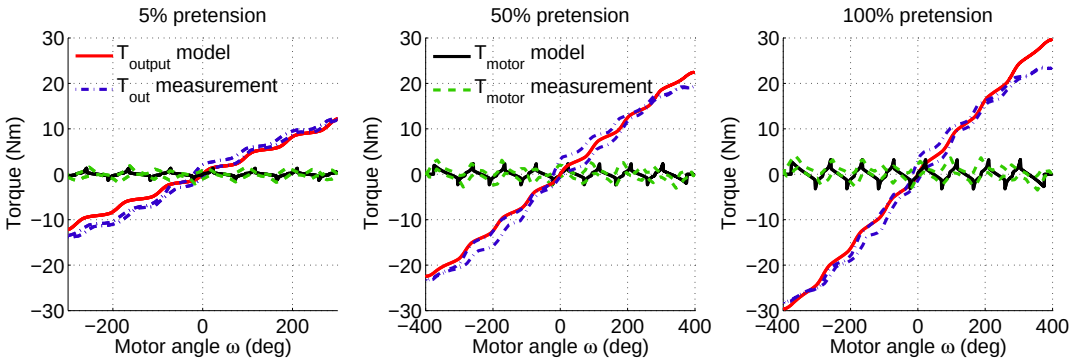

Fig. 9. The measurements endorse that the modeled output and motor torque are valid, and the stiffness can be altered. Furthermore, the lowered motor torque and variable load cancellation is clearly proven.

is installed, the T_{output} bandwidth is currently limited to 0.1 Hz. However, installing a more powerful DC motor, such as the DCX 32 L, with GPX 32 gearhead (ratio 1:16 and belt 1:4) will increase the torque bandwidth to 1 Hz while only increasing the weight with 0.3 kg. This is due to the inherent property of the SPEA that allows variable load cancellation. As such, the geartrain of a more powerful motor still only needs to deliver 5 Nm maximum which significantly reduces the weight of the required gearbox and motor, since the weight of the motor scales linear with the maximum torque it can deliver.

V. EXPERIMENTS

Firstly, the experiments are performed to verify the working principle of all components of the actuator. Multiple motor trajectories are imposed at varying speeds and pretension. The cylindrical cam mechanism proved to be working excellent. After numerous runs no problems are reported. The guides and tensioners performed well and no excessive wear is detected during normal working conditions. The guides could be improved slightly, by altering the design parameters, since in extreme equilibrium angles the outer spring unlocked occasionally. The other springs never unlocked. The pretensioning mechanism works fine, although a servomotor with a slightly higher stall torque is useful. The efficiency of the worm drive is most probably overestimated.

The motor is driven by a small Maxon ©EPOS2 24/2 drive with an ENX16 EASY feedback encoder for position control. Two additional US digital E6 optical encoders of 2000 counts per rotation are installed on the actuator. One to measure the angle between the input and the output link, and one to measure the rotation of the reeling rod to determine the pretension level. Data acquisition and motor drive control are performed on a National Instruments ©SB-RIO 9626 system via CANopen communication to the EPOS controller.

A blocked output experiment is performed to verify the actuator model, the variable stiffness and the variable load cancellation. The output angle is blocked at 0^o and the output force is measured to determine T_{output}. A Futek ©LSB 200 with 100 lb capacity is used, as shown on Fig. 7b, in combination with a CSG 110 a amplifier. The motor torque T_{motor} is estimated based on the motor current I_{motor} which is acquired from the EPOS2 via the CANopen line. A standard DC model based on the datasheet values of motor and gearbox is then used to determine T_{motor} from I_{motor}. The motor's viscous damping coefficient ν_m is approximated by the reported torque constant, no load current and no load speed.

The blocked output experiment consists of recruiting all springs from one side to the other, and in reverse. As such, the full output torque range is covered. In Fig. 9 T_{motor} and T_{output} are both shown as a function of the motor angle ω. The experiment is repeated for three pretension levels: 5%, 50% and 100%. Firstly, it is clear from the graph that T_{motor} and T_{output} clearly follow the model. The deviation for higher pretension in the first quadrant is due to a lack of rigidity in the blocking structure. Due to the variable load cancellation with 8 parallel springs T_{motor} is drastically (approximately $\frac{1}{8}$) lower than T_{output}. Furthermore, for different motor angles ω the motor torque is 0 Nm, which means the system is statically balanced. This means the energy consumption is 0 J while with a serial actuator current needs to be consumed to maintain T_{output}. For the same ω but an altered stiffness, T_{output} almost doubles, which means the stiffness doubles as well. T_{motor} increases for increased pretension.

In Fig. 10 T_{motor} is shown as a function of time. During this experiment, all springs are recruited to one side, where the maximum T_{output} is maintained for 3 sec, then all springs are recruited to the other side. Since the actuator consists of 8 parallel layers, T_{motor} consists of 8 peaks during recruitment of these springs. More specifically, each peak is actually similar to the one layer measurement in Fig 2. The modeled and measured T_{motor} are clearly similar. The magnitude of the measured values is slightly higher compared to the model, due some levels of unmodeled friction. The increased magnitude due to increased pretension can be observed in both measurements and model. One can observe that half of the peaks of T_{motor} are missing in the experiments, although in Fig.2 both positive and negative sides are represented. This is due to the fact that the devised model is a statical model. In Fig. 2 the experiment is conducted at very slow speeds, as such the statical model is valid. This is no longer true

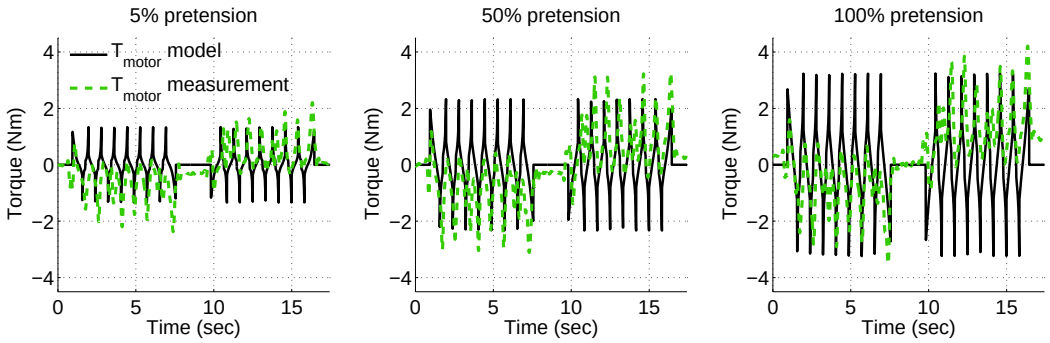

Fig. 10. The motor torque increases with increasing pretension. Due to unmodeled dynamic effects the measurements slightly deviate from the model.

for the experiment in Fig.10, therefor the measured profile deviates from the model. Another interesting aspect is the constant T_{motor} of nearly 0 Nm between 7 sec and 10 sec, since T_{output} during this period is 30 Nm. Since T_{motor} here is nearly 0 Nm, the energy consumption is negligible.

VI. CONCLUSIONS AND FUTURE WORK

This paper presents a cylindrical cam mechanism for unlimited subsequent spring recruitment. After an elaboration of the working principle, it is explained how the innovative mechanism is deployed in a MACCEPA-based SPEA. The actuator presented consists of 8 parallel MACCEPA layers with self-closing guides. The mechanism enables to consecutively recruit and lock the 8 parallel springs to provide an output torque up to 40 Nm. The experiments confirm that the variable load cancellation reduces the motor torque to maximum 5 Nm. Furthermore, the experiments confirmed that the actuator allows to vary the joint stiffness by 100%. The paper shows that the increased mechanical complexity can be overcome by inventive combination of traditional and additive manufacturing techniques. The actuator has a weight of 2.2 kg and height of 200 mm. The presented MACCEPA-based SPEA will be used as a test platform to further investigate the virtues of the SPEA, and test SPEA specific control strategies. In future work we aim to implement the SPEA actuators in robots for human-robot interaction, such as robotic co-workers.

REFERENCES

[1] B. Vanderborght, A. Albu-Schaeffer, A. Bicchi, E. Burdet, D. Caldwell, R. Carloni, M. Catalano, O. Eiberger, W. Friedl, G. Ganesh *et al.*, "Variable impedance actuators: A review," *Robotics and Autonomous Systems*, vol. 61, no. 12, pp. 1601–1614, 2013.

[2] A. Bicchi, G. Tonietti, M. Bavaro, and M. Piccigallo, "Variable stiffness actuators for fast and safe motion control," *International Journal of Robotics Research*, pp. 527–536, 2005.

[3] T. Lens, J. Kunz, O. v. Stryk, C. Trommer, and A. Karguth, "Biorob-arm: A quickly deployable and intrinsically safe, light- weight robot arm for service robotics applications," in *Robotics (ISR), 2010 41st International Symposium on and 2010 6th German Conference on Robotics (ROBOTIK)*, June 2010, pp. 1–6.

[4] S. Haddadin, A. Albu-Schaffer, O. Eiberger, and G. Hirzinger, "New insights concerning intrinsic joint elasticity for safety," in *IEEE/RSJ International Conference on Intelligent Robots and Systems (IROS)*, Oct 2010, pp. 2181–2187.

[5] B. Vanderborght, B. Verrelst, R. Van Ham, M. Van Damme, D. Lefeber, B. M. Y. Duran, and P. Beyl, "Exploiting natural dynamics to reduce energy consumption by controlling the compliance of soft actuators," *The International Journal of Robotics Research (IJRR)*, vol. 25, no. 4, pp. 343–358, 2006.

[6] L. Visser, R. Carloni, and S. Stramigioli, "Energy-efficient variable stiffness actuators," *IEEE Transactions on Robotics*, vol. 27, no. 5, pp. 865 –875, October 2011.

[7] P. Beckerle, J. Wojtusch, J. Schuy, B. Strah, S. Rinderknecht, and O. Stryk, "Power-optimized stiffness and nonlinear position control of an actuator with variable torsion stiffness," in *IEEE/ASME International Conference on Advanced Intelligent Mechatronics (AIM)*, July 2013, pp. 387–392.

[8] D. Braun, M. Howard, and S. Vijayakumar, "Optimal variable stiffness control: formulation and application to explosive movement tasks," *Autonomous Robots*, vol. 33, no. 3, pp. 237–253, 2012.

[9] G. Mathijssen, P. Cherelle, D. Lefeber, and B. Vanderborght, "Concept of a series-parallel elastic actuator for a powered transtibial prosthesis," *Actuators*, vol. 2, no. 3, pp. 59–73, 2013.

[10] H.-S. Kim and J.-B. Song, "Multi-dof counterbalance mechanism for a service robot arm," *Mechatronics, IEEE/ASME Transactions on*, vol. 19, no. 6, pp. 1756–1763, Dec 2014.

[11] N. Paine, S. Oh, and L. Sentis, "Design and control considerations for high-performance series elastic actuators," *IEEE/ASME Transactions on Mechatronics*, vol. 19, no. 3, pp. 1080–1091, June 2014.

[12] N. Tsagarakis, S. Morfey, H. Dallali, G. Medrano-Cerda, and D. Caldwell, "An asymmetric compliant antagonistic joint design for high performance mobility," in *IEEE/RSJ International Conference on Intelligent Robots and Systems (IROS)*, Nov 2013, pp. 5512–5517.

[13] J. Urata, Y. Nakanishi, K. Okada, and M. Inaba, "Design of high torque and high speed leg module for high power humanoid," in *IEEE/RSJ International Conference on Intelligent Robots and Systems (IROS)*, 2010, pp. 4497–4502.

[14] G. Mathijssen, D. Lefeber, and B. Vanderborght, "Variable recruitment of parallel elastic elements: Series-parallel elastic actuators (spea) with dephased mutilated gears," *IEEE Transactions on Mechatronics*, 2014 (in press), (Accepted 3 February 2013).

[15] G. Mathijssen, R. Furnmont, B. Brackx, R. Van Ham, D. Lefeber, and B. Vanderborght, "Design of a novel intermittent self-closing mechanism for a maccepa-based series-parallel elastic actuator (spea)," in *IEEE/RSJ International Conference on Intelligent Robots and Systems (IROS)*, 2014.

[16] R. Van Ham, B. Vanderborght, M. Van Damme, B. Verrelst, and D. Lefeber, "Maccepa, the mechanically adjustable compliance and controllable equilibrium position actuator: Design and implementation in a biped robot," *Robotics and Autonomous Systems*, vol. 55, no. 10, pp. 761–768, October 2007.

[17] J. Bickford, *Mechanisms for intermittent motion*. Industrial Press New York, 1972.

[18] J. Zhang, G. Song, G. Qiao, Z. Li, W. Wang, and A. Song, "A novel one-motor driven robot that jumps and walks," in *IEEE International Conference on Robotics and Automation (ICRA)*, 2013, pp. 13–19.

[19] S. Wolf, O. Eiberger, and G. Hirzinger, "The dlr fsj: Energy based design of a variable stiffness joints," in *IEEE International Conference on Robotics and Automation (ICRA)*, 2011, pp. 5082–5089.